STELLAR ASTROPHYSICS

An observed population of intermediate-mass helium stars that have been stripped in binaries

M. R. Drout[1,2]*†, Y. Götberg[2]*†, B. A. Ludwig[1], J. H. Groh[3], S. E. de Mink[4,5], A. J. G. O'Grady[1,6], N. Smith[7]

The hydrogen-rich outer layers of massive stars can be removed by interactions with a binary companion. Theoretical models predict that this stripping produces a population of hot helium stars of ~2 to 8 solar masses ($M_\odot$), however, only one such system has been identified thus far. We used ultraviolet photometry to identify potential stripped helium stars then investigated 25 of them using optical spectroscopy. We identified stars with high temperatures (~60,000 to 100,000 kelvin), high surface gravities, and hydrogen-depleted surfaces; 16 stars also showed binary motion. These properties match expectations for stars with initial masses of 8 to 25 $M_\odot$ that were stripped by binary interaction. Their masses fall in the gap between subdwarf helium stars and Wolf-Rayet stars. We propose that these stars could be progenitors of stripped-envelope supernovae.

Approximately 70% of massive stars [initial masses of >8 solar masses ($M_\odot$)] interact with a binary companion during their lifetimes (*1*, *2*). Those binary interactions are expected to strip the hydrogen-rich envelopes from many massive stars, leaving an exposed hot and compact helium core. The resulting stripped stars have sufficiently long lifetimes to be observed and are expected to be numerous (*3*).

Binary-stripped massive stars are expected to influence multiple astrophysical processes: They are thought to be the progenitors of most hydrogen-poor core-collapse supernovae (*4*–*6*). The neutron stars that have been observed in gravitational wave events are thought to have undergone two phases of envelope stripping (*7*). And the high surface temperatures of stripped stars make them potential sources of ionizing photons (*8*, *9*).

Despite their predicted ubiquity, few binary-stripped helium stars with masses between ~2 and 8 $M_\odot$—which are expected to be produced by stars with initial masses between ~8 and 25 $M_\odot$—have been found. Many other types of hydrogen-deficient stars have been observed (*10*). These are classified as high-mass Wolf-Rayet (WR) stars (*11*), low-mass subdwarfs (*12*), extreme helium stars (*13*), and central stars of planetary nebulae (*14*), all of which have been found in binary systems (*15*–*17*). However, none of those classes occupy the mass range that has been predicted to produce most stripped-envelope supernovae or neutron star mergers (*7*). Only one hot helium star with an appropriate mass has been reported: the "quasi-WR" star in the system HD 45166 (*18*, *19*).

If such systems are truly rare, models of binary evolution would need to be revised. Alternatively, there could be an observational bias: The optical flux from intermediate-mass stripped stars might be hidden by a bright main sequence (MS) companion star. Although helium star mass-loss rates are uncertain (*20*), they are predicted to exhibit weaker wind features than luminous WR stars, so they could potentially have eluded detection in previous surveys targeting those features (*21*).

Ultraviolet photometry

Some stripped helium star binaries might be detectable by excess ultraviolet (UV) emission in their spectral energy distributions (*22*). To assess this possibility, we calculated synthetic spectra for a large set of hypothetical binaries containing a stripped star and an MS star (*20*). We find that many of the hypothetical systems remain obscured by the brightness of the MS star, but hot intermediate-mass helium stars paired with MS companions of $\lesssim$10 $M_\odot$ occupy a specific region of UV-optical color-magnitude diagrams (CMDs): blueward of the MS at intermediate luminosities of –1 mag > M_{UVM2} > –4 mag (where M_{UVM2} is the absolute magnitude in the UVM2 ultraviolet filter; figs. S4 and S5).

We searched for massive stars with UV magnitudes that fall within the CMD region predicted by our synthetic spectra. We targeted stars in the Large Magellanic Cloud (LMC) and Small Magellanic Cloud (SMC) galaxies, because they contain a large number of massive stars at known distances, with low obscuration by dust. We measured UV photometry using archival images from the Swift Ultraviolet Survey of the Magellanic Clouds (*23*). These images cover ~3 square degrees of the SMC and ~9 square degrees of the LM[illegible] three UV filters at a resolution of 2.5 arc[illegible]. To reduce the effects of crowding at that resolution, we used the forward modeling code The Tractor (*24*) to perform forced point-spread function photometry. We adopted the known locations of stars in the optical Magellanic Cloud Photometric Survey (*25*, *26*), which has better spatial resolution.

This process determined UV magnitudes for >500,000 sources in the directions of the LMC and SMC (*20*). Figure 1 shows a UV-optical CMD of all the sources. We adopted distances of 50 and 61 kpc and visual dust extinctions A_V of 0.38 and 0.22 mag for the LMC and SMC, respectively (*20*). LMC and SMC extinction curves (*27*) were used to determine the corresponding dust obscuration in the UV. The CMD contains a dense band (which we ascribe to the MS) and multiple sources blueward of the MS, which we consider to be candidate stripped helium star binaries.

Optical spectroscopy

We selected 25 candidate systems for follow-up spectroscopy by choosing targets that have luminosities and colors consistent with our predictions for binaries containing intermediate-mass helium stars (*20*) (indicated in Fig. 1). The stars are of similar brightness to MS stars with initial masses of ~6 to 15 $M_\odot$ but—for the adopted extinction—are located blueward of the zero-age MS (ZAMS) in nine distinct UV-optical CMDs (*20*). They have UV-optical colors similar to those of WR stars but are intrinsically fainter. For some systems, the observed colors and magnitudes approach predictions for isolated helium stars with masses between ~2 and 8 $M_\odot$ (Fig. 1).

We obtained between 1 and 30 optical spectra for each system using the Magellan Echellette spectrograph (*28*) on the 6.5-m Magellan Baade telescope at Las Campanas Observatory, Chile. All 16 systems with more than one epoch show radial velocity variations, consistent with being binary systems (table S9).

We used kinematics to reject any likely foreground objects. All 25 systems have average radial velocities consistent with expectations for stars in the LMC and SMC (*20*). We combined these with proper motions (*29*), finding that 23 systems have three-dimensional motion that is consistent with known O-type and B-type massive stars in the LMC and SMC (*20*) (O-type stars typically have initial masses of $\gtrsim$15 $M_\odot$, and B-type stars typically have initial masses of ~2 to 15 $M_\odot$). The remaining two objects (stars 5 and 6 in table S9) show slight offsets in proper motion but have data quality issues in the proper motion catalog. We therefore retained them in our sample.

Figure 2A shows examples of the spectra; the full sample is provided in figs. S16 to S21. We classify the stars into three broad groups:

[1]David A. Dunlap Department of Astronomy and Astrophysics, University of Toronto, Toronto M5S 3H4, Canada. [2]The Observatories of the Carnegie Institution for Science, Pasadena, CA 91101, USA. [3]Independent researcher, 2314 Leiden, Netherlands. [4]Max-Planck-Institut für Astrophysik, 85741 Garching, Germany. [5]Anton Pannekoek Institute for Astronomy, University of Amsterdam, 1090 GE Amsterdam, Netherlands. [6]Dunlap Institute for Astronomy and Astrophysics, University of Toronto, Toronto M5S 3H4, Canada. [7]Steward Observatory, University of Arizona, Tucson, AZ 85721, USA.
*Corresponding author. Email: maria.drout@utoronto.ca (M.R.D.); ygoetberg@carnegiescience.edu (Y.G.)
†These authors contributed equally to this work.

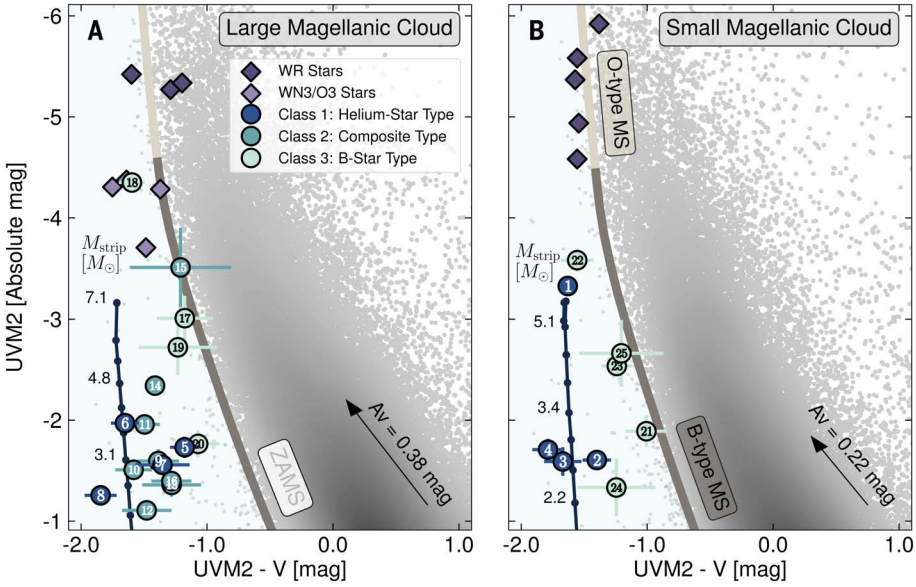

Fig. 1. Candidate stripped helium star binaries in UV-optical color-magnitude diagrams. Gray dots show absolute magnitude photometry in the UVM2 ultraviolet band as a function of the UVM2-V (where V is the visual band) color for stars in (**A**) the LMC and (**B**) the SMC. Numbered circles indicate the 25 stars we investigated further with optical spectroscopy (table S7), color coded according to their observed spectral morphologies (see legend). Error bars are 1σ. These systems have similar UV-optical colors, but lower brightnesses than either WR stars (dark-purple diamonds) (*48*, *49*) or the weaker-wind WN3/O3 stars (light-purple diamonds) (*36*). The connected black dots indicate models of isolated helium-core burning stripped stars, which are labeled with the current mass of the stripped star (M_{strip}) (*22*). The thick curved line indicates the expected position of the ZAMS for O-type (light gray) and B-type (dark gray) stars. All observed data have been corrected for dust extinction (indicated by the arrows), and all magnitudes are in the AB system.

1) Class 1 (eight stars): These spectra are dominated by absorption lines of He II. In some cases, lines of N IV and/or N V are visible in emission or absorption. These three ions are characteristic of very hot stars (*30*).

2) Class 2 (eight stars): These spectra show He II in absorption but also have strong absorption lines of hydrogen in the blue part of the spectrum (the short-wavelength Balmer lines). Six of these spectra also show He I; two do not, which indicates that the spectrum is a blend of two stars with different temperatures (*20*).

3) Class 3 (nine stars): No He II lines are visible in the optical spectrum. These spectra are dominated by strong Balmer and He I absorption lines, closely resembling those of B-type MS stars.

Interpretation of the spectra

The CMD locations and spectral morphologies of these 25 stars are consistent with our theoretical predictions for binary systems containing hot intermediate-mass helium stars. Our synthetic spectra of such objects (calculated above) show spectral features similar to those of WR stars, but with substantially weaker emission or absorption lines owing to their lower luminosities and mass-loss rates (*20*). In the set of helium star plus MS star composite spectral models, we identify the same three broad spectral classes as in our observations. Reproducing the absorption line spectra of the observed sample requires mass-loss rates for intermediate-mass helium stars that are at least an order of magnitude lower than extrapolations of WR mass loss (*20*), which is consistent with theoretical predictions (*31*).

We interpret the progression from class 3 to class 1 as an increasing contribution from the helium star to the optical flux of the system (*20*). Figure 2B compares the equivalent width (EW) of the He II λ5411 line as a function of Hη + He II λ3835 [where λ notation indicates the wavelengths in angstroms (Å), Hη is the seventh Balmer line, and + indicates blended lines] for both our observed sample and the composite models. The He II λ5411 line arises from the helium star; it is not expected at the cooler temperatures of B-type MS stars. We use the Hη + He II λ3835 blend to probe the presence of an MS companion, because strong short-wavelength Balmer lines are not expected in hot hydrogen-depleted stars [we have to use a blended line because our synthetic spectra show no isolated hydrogen lines in the optical range for these stars (*20*)]. In this parameter space, all 25 observed stars overlap with the predictions from the composite models, regardless of which helium star mass-loss rates are adopted (*20*).

For class 3 stars, we find 3σ upper limits on the EW of He II λ5411 of $\lesssim$0.2 Å (table S8). This corresponds to models where the helium star contributes <20% of the optical flux, and hence the spectra appear like those of B-type MS stars. Although such stars can show a UV excess, our models predict that they should be close to the ZAMS (as observed for the class 3 stars in Fig. 1). In contrast, the class 1 stars all have Hη + He II λ3835 EWs of <1.2 Å, consistent with models for systems where a helium star contributes >80% of the optical flux, so the spectra appear like those of isolated helium stars. The models only produce such spectra when the MS companion has a mass of $\lesssim 3.5\,M_\odot$. We infer that the class 1 objects either (i) come from binary systems where the two stars had very different initial masses; or (ii) have companions that are compact objects (neutron stars or black holes), not MS stars. Those systems would also have sufficiently blue colors to match the observations; in the CMD, they are close to models of isolated helium stars. Although dust extinction toward individual objects is uncertain, the location of these models in the CMD is similar to that of the class 1 objects (Fig. 1). The intermediate class 2 stars fall close to models where the helium star contributes 20 to 80% of the optical flux, so they have composite optical spectra with contributions from both stars.

Estimates of stellar properties

To assess the nature of the hot stars in these systems, we considered EW diagnostics that distinguish the optical spectra of stripped stars from MS stars and estimate their surface properties. We used the 1D nonlocal thermodynamic equilibrium radiative transfer code CMFGEN (*32*) to compute a set of spectral models with a range of effective temperatures (30 kK ≤ T_{eff} ≤ 100 kK, where kK is kilokelvin), surface gravities [4.0 < log(g/cm s^{-2}) < 6.0], and surface hydrogen mass fractions ($X_{H,surf}$ = 0.01, 0.1, 0.3, and 0.5, which are all depleted below MS values) (*20*). We choose a baseline mass-loss rate of $10^{-9} M_\odot$ year^{-1} because it produces absorption line spectra. We then tested the impact of this choice on our results by varying the assumed mass-loss rate by two orders of magnitude. These models cover a broad parameter space without making assumptions about the detailed evolutionary state of each system. Figure 3 shows these models compared with both the class 1 stars and O- and B-type MS model spectra (*33*, *34*) in three parameter spaces. We focused on the class 1 stars because we expect them to have minimal contamination from any companion.

To constrain the effective temperatures of these stars, Fig. 3A shows the EW of He II λ5411 as a function of the EW of He I λ5876, which provides a temperature diagnostic due to variations in the the helium ionization balance

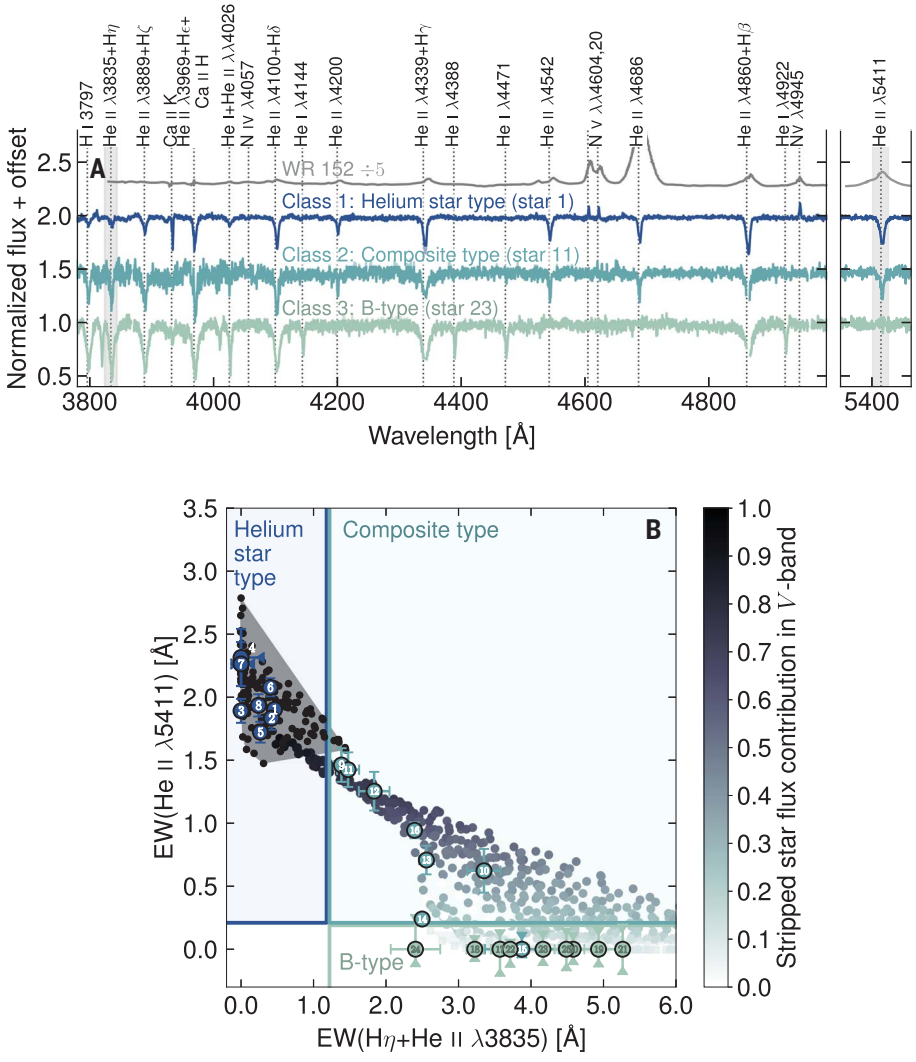

Fig. 2. Optical spectra with three spectral morphologies. (**A**) Three example observed spectra (colored lines) classified as class 1, 2, or 3 (see text), offset for display. Spectra of all the other stars in our sample are shown in figs. S16 to S21. The gray line shows the optical spectrum of an example WR star (WR 152 divided by a factor of 5) for comparison (*50*); it has similar line transitions as the class 1 stars, but in emission. Vertical dotted lines indicate locations of spectral lines, which are identified by the labels above. Gray shaded bands indicate the lines used in (B). (**B**) EWs of He II λ5411 and Hη + He II λ3835 for all 25 stars in our spectroscopic sample (large numbered circles). T-shaped error bars indicate 1σ uncertainties on detected lines; triangle-terminated error bars indicate 3σ upper or lower limits (for absorption or emission) on undetected lines. For comparison, we show synthetic models of single stripped stars (black dots enclosed in the gray shaded region), single B-type MS stars (light-green squares), and composites of the two (colored dots). Model equivalent widths were calculated assuming a signal-to-noise ratio of 35, consistent with the median signal-to-noise of the observed stars (*20*). Models are colored to indicate the fraction of *V*-band flux contributed to the binary by the stripped star (color bar). Shaded and labeled boxes define the three classes of spectral morphology we identify; observed data points use the same colors as the shading. Star 15 does not exhibit He II λ5411 but does show He II λ4686, so we classify it as class 2 (*20*). The observed sample forms a sequence that overlaps with the theoretical predictions for stripped helium star binaries.

with temperature. For all but two stars, we find $T_{\rm eff}$ > 70 kK owing to the lack of detected He I; those are temperatures typical of WR stars, higher than the hottest O-type stars (*35*). For some objects, the detection of N IV and/or N V can provide an alternative temperature estimate, which ranges between ~70 to 80 kK and ≳90 kK (fig. S11) (*20*).

Figure 3B shows an equivalent plot for the EWs of He II λ3835 + Hη and He II λ4860 + Hβ. This provides a rough estimate of surface gravity, because of the decrease in line strength relative to the observed pseudo-continuum for short-wavelength Balmer lines as they broaden as a result of increasing log(*g*). The observed sample is consistent with surface gravities log(*g*) ≳ 5, higher than is observed in MS stars.

Figure 3C shows the pure helium blend He I + He II λ4026 as a function of the hydrogen/helium blend He II + Hδ λ4100, which probe the hydrogen and helium surface mass fractions. The observed stars are all consistent with hydrogen-depleted surfaces, spanning the location of the model grid from $X_{\rm H,surf}$ = 0.01 (almost hydrogen-free) to $X_{\rm H,surf}$ = 0.3. We chose these diagnostics to avoid more wind-sensitive spectral lines. Our tests with different assumptions for the mass-loss rate and wind velocity do not change these results (*20*).

The properties we estimated for each star are listed in table S2. These diagnostics indicate that the class 1 stars are hot, compact, and hydrogen-poor. Figure 1 shows that their brightnesses fall along a sequence, connecting WR stars and the slightly lower luminosity WN3/O3 stars (*36*) to subdwarfs. Figure S13 shows that this sequence also appears in the strengths of stellar wind lines in the optical spectra.

Figure 4 compares our derived constraints on $T_{\rm eff}$ and log(*g*) with predictions for intermediate-mass helium stars (*22*). The observed stars have surface gravities between those of MS stars and white dwarfs—consistent with our expectations for helium stars—and temperatures hotter than most subdwarf stars (*37*). Figure 4 also shows a set of evolutionary tracks (*22*). The observed stars are consistent with predictions for the core-helium burning phase of ~2.5 to 8 $M_\odot$ stripped stars, which have progenitors with initial masses of between ~9 and 25 $M_\odot$. These ranges are high enough for the stars to later undergo core collapse (*38*), so they will explode as stripped-envelope supernovae (*39*). The winds from stars with initial masses of <25 $M_\odot$ are too weak to remove the hydrogen-rich envelope (*40*), so binary interaction is thought to be the primary mechanism for stripping stars in that mass range (see supplementary text section of the supplementary materials).

Excluding alternative explanations

We considered other possible interpretations of the stars in our sample (see supplementary text). Some of the class 3 stars could be ordinary (B-type) MS stars in regions with very little dust obscuration; in this case, they would appear to show a UV excess resulting from an overcorrection of the photometry. However, the same is not true for the class 1 and class 2 stars, whose locations on the CMD (Fig. 1) are inconsistent with massive O-type MS stars (the only type of MS star expected to have detectable He II) for any extinction values. The absorption-line spectral morphologies of the class 1 and class 2 stars are also distinct from those of WR stars (Fig. 2A).

Other types of stars can reach very high temperatures and similar brightnesses, such as accreting white dwarfs, central stars of planetary

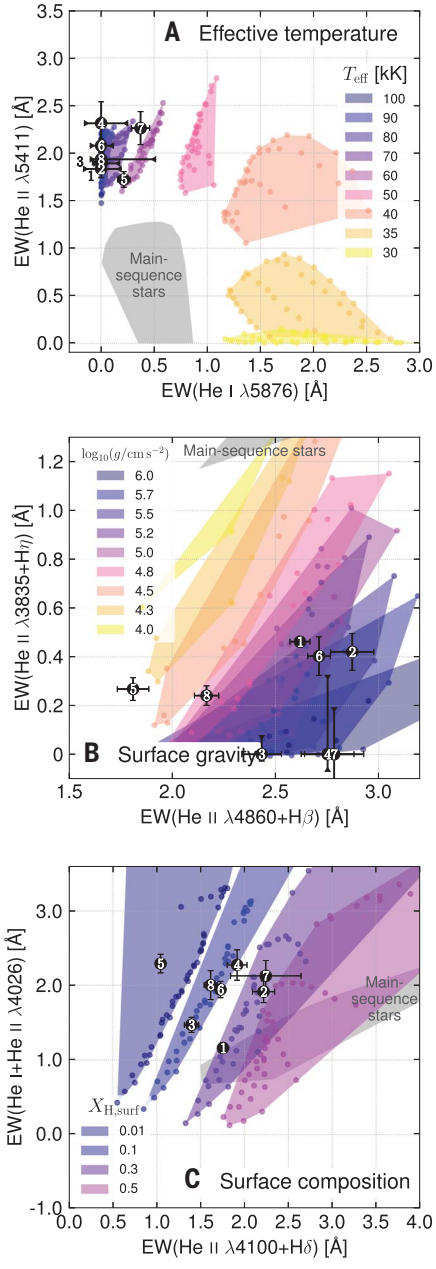

Fig. 3. Diagnostic diagrams used to estimate stellar properties. Each panel plots EWs of pairs of spectral lines (or line blends), chosen to constrain (**A**) effective temperature, (**B**) surface gravity, and (**C**) helium enrichment. Black data points (with 1σ error bars) show the measured EWs for the eight class 1 stars, which have helium star–type spectra. Colored dots show predictions from a grid of model spectra, with properties indicated by color (see legends; shaded regions encompass the full range for each value). Model equivalent widths were calculated assuming a signal-to-noise of 100, consistent with the median signal-to-noise of the observed class 1 stars (*20*). Gray shaded regions indicate MS star models (*20*). As shown in (A), all the class 1 stars have an effective temperature of >50 kK, so we only show models with $T_{\rm eff} \geq 50$ kK and O-type MS models in (B) and (C). The class 1 stars are hot, compact, hydrogen-poor, and do not overlap MS stars.

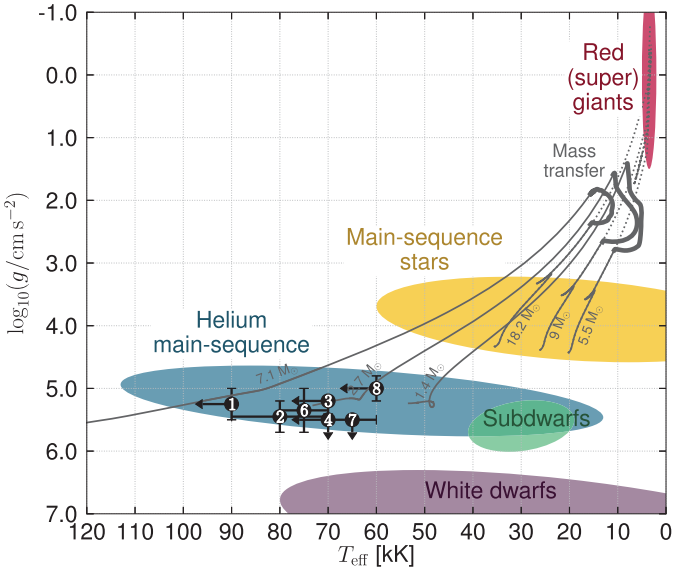

Fig. 4. Physical properties of the eight class 1 systems compared with other types of stars. Estimated effective temperatures and surface gravities of the class 1 stars are shown as numbered black circles. Error bars and limits correspond to the properties of the models that the star overlaps with in Fig. 3 and are listed in table S2. Colored ellipses indicate the regions occupied by main-sequence stars (yellow), white dwarfs (purple), theoretical predictions for helium stars fusing helium in the center (the helium main-sequence, blue), subdwarfs (green), and red giants and supergiants (red). Black lines show evolutionary tracks for stars with ZAMS masses of 5.5, 9.0, and 18.2 $M_\odot$, starting on the main sequence and extending until the end of central helium burning (*20*). Single stars of these masses (dotted lines) would evolve into cool and extended red giants or red supergiants. Binary stars of these initial masses undergo envelope stripping by means of mass transfer (thick solid lines) and subsequently evolve to burn helium as hot and compact helium stars with stripped masses of 1.4, 2.7, and 7.1 $M_\odot$ (thin solid lines). These stripped helium stars have surface properties similar to our observed sample.

nebulae, and very young post-asymptotic giant branch (post-AGB) stars (*10*), but those types all have circumstellar material, which produces emission lines or an infrared excess (*41*, *42*), neither of which we observe. Young post-AGB stars are also expected to be very rare (see supplementary text). Very fast rotation could fully mix stars—resulting in hot and compact helium stars—but this is only expected at higher masses and luminosities (*43*). Some hot low-mass objects (such as evolved subdwarfs and white dwarf merger products) could pollute our sample, but our targeting of the LMC and SMC means that they would need to be foreground objects located in the halo of the Milky Way. By examining the frequency of UV excesses in a control sample, we predict that there are <1 foreground objects along the line of sight to the LMC or SMC with colors, magnitudes, and kinematics similar to our spectroscopic sample (see supplementary text).

The properties we infer for the observed stars differ from previously identified helium-rich stars. They are much hotter and more compact than cool helium giants, such as the star ν Sgr [$T_{\rm eff} \lesssim 15$ kK, $\log(g) \sim 2$] (*44*, *45*). While the mass of ν Sgr is uncertain (*46*), it could be in a subsequent evolutionary phase; some stripped stars expand substantially upon completion of core-helium burning (*47*). The surface properties we estimated for the class 1 stars are similar to those of HD 45166, but their spectra are distinct, with HD 45166 having a spectrum dominated by emission lines. This indicates that the anomalously slow wind speed observed in HD 45166 might not be common (see supplementary text). Instead, the absorption spectra of stars in our sample imply low mass-loss rates, consistent with theoretical predictions (*20*).

The properties, binary companions, and evolutionary history of the individual systems in our sample are likely diverse. Nevertheless, we conclude that they constitute a population of massive stars stripped through binary interaction. Because only a subset of stripped star binaries are expected to show a UV excess (*20*), the population we observe represents only a small fraction of the predicted intermediate-mass helium stars. Many other examples could be hidden by brighter companion stars. With estimated masses of ~2 to 8 $M_\odot$, the stars we observed fill a gap in previously identified helium stars, connecting subdwarfs with WR stars.

REFERENCES AND NOTES

1. H. Sana *et al.*, *Science* **337**, 444–446 (2012).
2. M. Moe, R. Di Stefano, *Astrophys. J. Suppl. Ser.* **230**, 15 (2017).
3. Y. Shao, X.-D. Li, *Astrophys. J.* **908**, 67 (2021).
4. J. D. Lyman *et al.*, *Mon. Not. R. Astron. Soc.* **457**, 328–350 (2016).
5. N. Smith, W. Li, A. V. Filippenko, R. Chornock, *Mon. Not. R. Astron. Soc.* **412**, 1522–1538 (2011).
6. J. J. Eldridge, M. Fraser, S. J. Smartt, J. R. Maund, R. M. Crockett, *Mon. Not. R. Astron. Soc.* **436**, 774–795 (2013).
7. T. M. Tauris *et al.*, *Astrophys. J.* **846**, 170 (2017).
8. E. R. Stanway, J. J. Eldridge, G. D. Becker, *Mon. Not. R. Astron. Soc.* **456**, 485–499 (2016).
9. Y. Götberg *et al.*, *Astron. Astrophys.* **634**, A134 (2020).
10. C. S. Jeffery, in *Hydrogen-Deficient Stars*, A. Werner, T. Rauch, Eds., vol. 391 of *Astronomical Society of the Pacific Conference Series* (Astronomical Society of the Pacific, 2008), pp. 3–16.
11. P. A. Crowther, *Annu. Rev. Astron. Astrophys.* **45**, 177–219 (2007).
12. U. Heber, *Publ. Astron. Soc. Pac.* **128**, 082001 (2016).

13. C. S. Jeffery, in *Hydrogen-Deficient Stars*, A. Werner, T. Rauch, Eds., vol. 391 of *Astronomical Society of the Pacific Conference Series* (Astronomical Society of the Pacific, 2008), pp. 53–63.
14. W. A. Weidmann, R. Gamen, *Astron. Astrophys.* **526**, A6 (2011).
15. L. Wang *et al*., *Astron. J.* **161**, 248 (2021).
16. M. M. Shara *et al*., *Mon. Not. R. Astron. Soc.* **464**, 2066–2074 (2017).
17. M. H. van Kerkwijk *et al*., *Nature* **355**, 703–705 (1992).
18. J. H. Groh, A. S. Oliveira, J. E. Steiner, *Astron. Astrophys.* **485**, 245–256 (2008).
19. T. Shenar *et al*., *Science* **381**, 761–765 (2023).
20. Materials and methods are available as supplementary materials.
21. P. Massey, K. F. Neugent, N. Morrell, D. J. Hillier, *Astrophys. J.* **788**, 83 (2014).
22. Y. Götberg *et al*., *Astron. Astrophys.* **615**, A78 (2018).
23. L. M. Z. Hagen *et al*., *Mon. Not. R. Astron. Soc.* **466**, 4540–4557 (2017).
24. D. Lang, D. W. Hogg, D. J. Schlegel, *Astron. J.* **151**, 36 (2016).
25. D. Zaritsky, J. Harris, I. B. Thompson, E. K. Grebel, P. Massey, *Astron. J.* **123**, 855–872 (2002).
26. D. Zaritsky, J. Harris, I. B. Thompson, E. K. Grebel, *Astron. J.* **128**, 1606–1614 (2004).
27. K. D. Gordon, G. C. Clayton, K. A. Misselt, A. U. Landolt, M. J. Wolff, *Astrophys. J.* **594**, 279–293 (2003).
28. J. L. Marshall *et al*., *Proc. SPIE* **7014**, 701454 (2008).
29. Gaia Collaboration, *Astron. Astrophys.* **674**, A1 (2023).
30. R. O. Gray, C. J. Corbally, *Stellar Spectral Classification*, Princeton Series in Astrophysics (Princeton Univ. Press, 2009).
31. J. S. Vink, *Astron. Astrophys.* **607**, L8 (2017).
32. D. J. Hillier, D. L. Miller, *Astrophys. J.* **496**, 407–427 (1998).
33. T. Lanz, I. Hubeny, *Astrophys. J. Suppl. Ser.* **146**, 417–441 (2003).
34. T. Lanz, I. Hubeny, *Astrophys. J. Suppl. Ser.* **169**, 83–104 (2007).
35. N. R. Walborn *et al*., *Astron. J.* **123**, 2754–2771 (2002).
36. K. F. Neugent, P. Massey, D. J. Hillier, N. Morrell, *Astrophys. J.* **841**, 20 (2017).
37. J. S. Drilling, C. S. Jeffery, U. Heber, S. Moehler, R. Napiwotzki, *Astron. Astrophys.* **551**, A31 (2013).
38. T. Ertl, S. E. Woosley, T. Sukhbold, H. T. Janka, *Astrophys. J.* **890**, 51 (2020).
39. S.-C. Yoon, L. Dessart, A. Clocchiatti, *Astrophys. J.* **840**, 10 (2017).
40. E. R. Beasor, B. Davies, N. Smith, *Astrophys. J.* **922**, 55 (2021).
41. H. Van Winckel, *Annu. Rev. Astron. Astrophys.* **41**, 391–427 (2003).
42. W. R. Hamann, M. Peña, G. Gräfener, M. T. Ruiz, *Astron. Astrophys.* **409**, 969–982 (2003).
43. I. Brott *et al*., *Astron. Astrophys.* **530**, A115 (2011).
44. D. Schoenberner, J. S. Drilling, *Astrophys. J.* **268**, 225–227 (1983).
45. T. Kipper, V. G. Klochkova, *Balt. Astron.* **21**, 219–240 (2012).
46. A. Gilkis, T. Shenar, *Mon. Not. R. Astron. Soc.* **518**, 3541–3555 (2023).
47. E. Laplace, Y. Götberg, S. E. de Mink, S. Justham, R. Farmer, *Astron. Astrophys.* **637**, A6 (2020).
48. J. Breysacher, M. Azzopardi, G. Testor, *Astron. Astrophys. Suppl. Ser.* **137**, 117–145 (1999).
49. P. Massey, A. S. Duffy, *Astrophys. J.* **550**, 713–723 (2001).
50. W.-R. Hamann, L. Koesterke, U. Wessolowski, *Astron. Astrophys. Suppl. Ser.* **113**, 459–471 (1995).
51. M. R. Drout *et al*., An observed population of intermediate-mass helium stars that have been stripped in binaries – theoretical, computational and observational data, Zenodo (2023); https://doi.org/10.5281/zenodo.7600727.
52. Y. Götberg *et al*., Stellar properties of observed stars stripped in binaries in the Magellanic Clouds – spectral models, Zenodo (2023); https://doi.org/10.5281/zenodo.7976200.
53. M. R. Drout *et al*., An observed population of intermediate-mass helium stars that have been stripped in binaries – raw spectroscopic data, Zenodo (2023); https://doi.org/10.5281/zenodo.10035849.

ACKNOWLEDGMENTS

We thank K. Auchettl, K. Breivik, C. Burns, A. Carpenter, J. Fuller, B. Hovis-Afflerbach, A. Ji, C. Johnston, D. Kelson, M. van Kerkwijk, D. Lang, C. Norman, T. Piro, M. Renzo, A. Roc, P. Senchyna, S. Torres, and M. Zapartas for fruitful discussions and support, and we acknowledge feedback from the anonymous referees that improved this manuscript. This paper includes data gathered with the 6.5 m Magellan Telescopes located at Las Campanas Observatory, Chile. We thank J. Mulchaey (Carnegie Observatories director), L. Infante (Las Campanas Observatory director), and the entire Las Campanas staff for their hard work and dedication to keeping the observatory operating through the COVID-19 pandemic, when a large fraction of this data was obtained. Computing resources used for this work were made possible by a grant from the Ahmanson Foundation. **Funding:** M.R.D. acknowledges support from the NSERC through grant RGPIN-2019-06186, the Canada Research Chairs Program, the Canadian Institute for Advanced Research (CIFAR), and the Dunlap Institute at the University of Toronto. Y.G. was supported by NASA through the NASA Hubble Fellowship Program grant HST-HF2-51457.001-A awarded by the Space Telescope Science Institute, which is operated by the Association of Universities for Research in Astronomy, Inc., for NASA, under contract NAS5-26555. A.J.G.O. acknowledges support from the Lachlan Gilchrist Fellowship Fund. S.E.d.M. acknowledges funding by the Netherlands Organization for Scientific Research (NWO) as part of the Vidi research program BinWaves under project number 639.042.728. N.S. was supported by NASA through HST grant GO-15824. **Author contributions:** M.R.D., S.E.d.M., and Y.G. designed the UV-optical color-magnitude diagrams used for candidate identification. M.R.D. and B.A.L. performed photometry on the Swift UVOT images and selected candidate targets for follow-up. M.R.D., Y.G., B.A.L., and A.J.G.O. performed the spectroscopic observations with the Magellan Baade telescope. M.R.D. reduced and analyzed the spectroscopic data and performed the kinematic analysis. Y.G. computed the spectral models with CMFGEN with input from J.H.G. and designed the equivalent width diagnostics used to estimate stellar properties. M.R.D. and Y.G. interpreted the observed sample in the context of the stellar models. M.R.D. and Y.G. wrote the paper, with input from B.A.L., J.H.G., S.E.d.M., A.J.G.O., and N.S. **Competing interests:** The authors have no competing interests to declare. **Data and materials availability:** Reduced and combined spectra of the 25 stars in our spectroscopic sample, our stripped helium star models, our main-sequence spectral models, equivalent width measurements from the theoretical models, and the index files used for astrometry are archived at Zenodo (*51*, *52*). The UV and optical photometry for the observed stars and models are provided in tables S6, S4, and S7 and are archived in machine-readable form at Zenodo (*51*). Raw Magellan Echellette spectra are also archived at Zenodo (*53*).

SUPPLEMENTARY MATERIALS

science.org/doi/10.1126/science.ade4970
Materials and Methods
Supplementary Text
Figs. S1 to S21
Tables S1 to S9
References (*54*–*167*)

Submitted 30 August 2022; accepted 27 October 2023
10.1126/science.ade4970